Journal of Contaminant Hydrology 216 (2018) 1–9

Contents lists available at ScienceDirect

Journal of Contaminant Hydrology

journal homepage: www.elsevier.com/locate/jconhyd

# The impact of water saturation on the infiltration behaviour of elemental mercury DNAPL in heterogeneous porous media

Andrea D'Aniello[a,*], Niels Hartog[b,c], Thomas Sweijen[c], Domenico Pianese[a]

[a] University of Naples Federico II, Department of Civil, Architectural and Environmental Engineering, via Claudio 21, 80125 Napoli, Italy
[b] KWR Watercycle Research Institute, Groningenhaven 7, Nieuwegein, The Netherlands
[c] Utrecht University, Department of Earth Sciences, Environmental Hydrogeology Group, Princetonplein 9, 3584 CC, Utrecht, The Netherlands

ARTICLE INFO

*Keywords:*
Elemental mercury
DNAPL
Unsaturated
Multiphase flow
Dual gamma ray

ABSTRACT

Industrial use has led to the presence of liquid elemental mercury ($Hg^0$) worldwide in the subsurface as Dense NonAqueous Phase Liquid (DNAPL), resulting in long lasting sources of contamination, which cause harmful effects on human health and detrimental consequences on ecosystems. However, to date, insight into the infiltration behaviour of elemental mercury DNAPL is lacking. In this study, a two-stage flow container experiment of elemental mercury DNAPL infiltration into a variably water saturated stratified sand is described. During the first stage of the experiment, 16.3 ml of liquid $Hg^0$ infiltrated and distributed into an initially partially water saturated system. Afterwards, during the second stage of the experiment, consisting of the simulation of a "rain event" to assess whether the elemental mercury already infiltrated could be mobilized due to local increases in water saturation, a significant additional infiltration of 4.7 ml of liquid mercury occurred from the remaining DNAPL source. The experiment showed that, under conditions similar to those found in the field, $Hg^0$ DNAPL infiltration is likely to occur via fingers and is strongly controlled by porous medium structure and water saturation. Heterogeneities within the porous medium likely determined preferential pathways for liquid $Hg^0$ infiltration and distribution, as also suggested by dual gamma ray measurements. Overall, this study highlights that the infiltration behaviour of mercury DNAPL is strongly impacted by water saturation. In the field, this may result in a preferential infiltration of $Hg^0$ DNAPL in wetter areas or in its mobilization due to wetting during a rain event, as indicated by this study, or a groundwater table rise. This should be considered when assessing the likely distribution pathways of historic mercury DNAPL contamination as well as the remediation efforts.

## 1. Introduction

Mercury is a contaminant of global concern as it causes harmful effects on human health and detrimental consequences on ecosystems (US EPA, 2007; World Chlorine Council, 2011). As a result of natural processes and anthropogenic activities, mercury is ubiquitous in the environment (Risher, 2003). Mercury release in ecosystems can result from a variety of anthropogenic sources like mercury mining (UNEP, 2002), mercury amalgamation for gold and silver mining (Lechler et al., 2000; UNEP, 2002; Hylander and Meili, 2003), and from industrial activities, such as wood preservation (Bollen et al., 2008), chlor-alkali facilities and thermometer manufacturing plants (Biester et al., 2002; Hylander and Meili, 2003; Bernaus et al., 2006; Arbestain et al., 2009; Brooks and Southworth, 2011; Miller et al., 2013). In particular, the chlor-alkali industry is among the principal appliers of mercury as well as the most important producer of wastes containing mercury (Pirrone et al., 2010). In 1996, almost 40% of the mercury produced in the World was used in the chlor-alkali industry (Sznopek and Goonan, 2000). In recent years, efforts have been made to control and further reduce mercury emissions into the environment, and legislative texts and government policies, like the United Nations Environmental Programme (UNEP) Global Mercury Convention (Minamata Convention on Mercury, 2013), are restricting its industrial use (NICOLE, 2015).

The occurrence of liquid elemental mercury in the subsurface as Dense NonAqueous Phase Liquid (DNAPL) has been reported worldwide in proximity of several chlor-alkali plants like in Lavaca Bay, Texas (USA), (Scanlon et al., 2005), near the Onondaga Lake, New York (USA), where it was found 17 m below the ground level (Deeb et al., 2011; ITRC, 2012), at the Oak Ridge Y-12 National Security Complex, Tennessee (USA), where the estimated loss of liquid $Hg^0$ to the soil is about 193,000 kg (Brooks and Southworth, 2011), at the Botany Industrial Park, Sydney (Australia), (Golder Associates, 2011), and at a

* Corresponding author.
*E-mail address:* andrea.daniello@unina.it (A. D'Aniello).

https://doi.org/10.1016/j.jconhyd.2018.07.006
Received 8 January 2018; Received in revised form 3 July 2018; Accepted 12 July 2018
Available online 17 July 2018
0169-7722/ 

former plant in the Netherlands (Sweijen et al., 2014). Once $Hg^0$ DNAPL infiltrates in the subsurface and immobilizes, it acts as a long lasting source of mercury contamination (Davis et al., 1997). In addition, liquid mercury may be subjected to speciation (Leterme and Jacques, 2013; González-Fernández et al., 2014; Leterme et al., 2014) and methylation (Compeau and Bartha, 1985; Gilmour et al., 1992), thus releasing in the water phase organic and inorganic mercury compounds that are more toxic, mobile, and soluble than $Hg^0$ itself. Furthermore, the volatilization of liquid elemental mercury also contributes to the spread of mercury through the environment (Walvoord et al., 2008).

Despite the worldwide importance and presence of liquid elemental mercury in the subsurface, only recently its DNAPL behaviour in porous media has been addressed. As for more extensively studied DNAPLs, such as creosote, carbon tetrachloride, trichloroethylene (TCE), and tetrachloroethylene (PCE), liquid elemental mercury requires to overcome an entry head to infiltrate in fully water saturated porous media (Devasena and Nambi, 2010), and it has a relatively high capacity to infiltrate as illustrated by numerical simulations (Sweijen et al., 2014; D'Aniello et al., 2018b) and by capillary pressure-saturation, $P_c(S)$, experiments under stable flow behaviour (D'Aniello et al., 2018a). However, in contrast with other DNAPLs, liquid elemental mercury was found to behave as a nonwetting phase with respect to both air and water, and therefore it requires to overcome an entry head to infiltrate in partially water saturated porous media (D'Aniello et al., 2018a). Moreover, as shown by $P_c(S)$ experiments performed under stable flow behaviour (D'Aniello et al., 2018a), liquid elemental mercury entry head in partially water saturated porous media is even higher than for fully water saturated conditions.

In the field, however, infiltration of elemental mercury DNAPL is expected to occur under unstable flow behaviour. Therefore, this study focussed on exploring the unstable flow behaviour of elemental mercury DNAPL in variably water saturated porous media. To this aim, a two-stage flow container experiment in a variably water saturated stratified sand was performed. To allow a quantitative analysis of $Hg^0$ DNAPL infiltration and distribution behaviour, non-intrusive measurements of porosity, water and $Hg^0$ saturations were performed with a dual gamma ray apparatus.

## 2. Materials and methods

### 2.1. Porous media and fluids

Filtersand 0.2–0.5 mm and Silversand S60, (FILCOM-Sibelco Group, 2015), were used as granular materials. Based on Wentworth classification (1922), the two sands are classified as medium sands and will be referred to as *medium sand 1* (MS1) and *medium sand 2* (MS2). For both sands, the intrinsic permeability (Table 1) was obtained experimentally (D'Aniello et al., 2018a) by means of the falling head method (Bear, 1972).

Demineralized water was used as the wetting fluid, and 99.9 + % redistilled liquid elemental mercury ($Hg^0$), (Alfa Aesar), was used as the nonwetting fluid (Table 2).

Elemental mercury entry heads for fully and partially water saturated systems (Table 3) were derived with the graphical method (Sillers et al., 2001; Pasha et al., 2015) based on the capillary pressure-saturation, $P_c(S)$, experiments, performed under stable flow behaviour, described in D'Aniello et al. (2018a).

**Table 1**
Porous Media Properties.

| Porous Medium | Median Particle Diameter (mm) | Particles Size Range (mm) | Porosity | [a]Intrinsic Permeability ($10^{-7}$ cm$^2$) |
|---|---|---|---|---|
| Medium Sand 1 | 0.39 | 0.200–0.500 | 0.368 | 1.61 |
| Medium Sand 2 | 0.26 | 0.125–0.355 | 0.391 | 1.79 |

[a] Number of measurements = 4 (details in D'Aniello et al., 2018a).

**Table 2**
Fluids Properties.

| Parameter | Unit | $Hg^0$ | Water |
|---|---|---|---|
| Density | g/cm$^3$ | 13.5[a] | 0.998 |
| Dynamic Viscosity | $10^{-3}$ Pa·s | 1.55[b] | 0.98 |
| Surface Tension | Dynes/cm | 485[c] | 72 |
| Interfacial Tension with Water | Dynes/cm | 375[b]-415[c] | – |

[a] CRC (2014);
[b] US DOE (2001) and references therein;
[c] Adamson and Gast (1997).

**Table 3**
$Hg^0$ DNAPL Entry Heads in MS1 and MS2 (details in D'Aniello et al., 2018a).

| Sample | System | Porosity | Initial Water Saturation | Entry Head (cm of $Hg^0$) |
|---|---|---|---|---|
| MS1 | $Hg^0$-Water | 0.354 | 1 | 6.19 |
| MS2 | $Hg^0$-Water | 0.375 | 1 | 12.51 |
| MS1 | $Hg^0$-Air-Water | 0.359 | 0.602 | 10.45 |
| MS2 | $Hg^0$-Air-Water | 0.373 | 0.502 | 15.74 |

### 2.2. Flow container experiment

The $Hg^0$ DNAPL infiltration experiment was performed in a Poly-Methyl Methacrylate (PMMA) flow container (Fig. 1).

The walls thickness was specifically designed and set to 1.5 cm to prevent any deformations. In addition, the back and front walls were layered with a glass plate of 0.5 cm, resulting in an inner thickness of the container of 3.95 cm. PMMA and glass were chosen as liquid $Hg^0$ is nonwetting with respect to these materials. To maintain constant air pressure within the container, the PMMA lid put on the top of the container was constructed with a ventilation hole.

The flow container was mainly filled with MS1 and, to study the effects of macro heterogeneities on $Hg^0$ migration, a layer of 5 cm height of MS2 was located 9 cm from the top of the upper MS1 layer (Fig. 1), resulting in a total height of the system of 25 cm. Two PMMA inlet walls, of 1 cm thickness, were added to create an undisturbed location for the liquid $Hg^0$ reservoir. To avoid relative displacements between the two screens and to fix them at the desired distance, the inlet walls were hooked on the front walls of the container and were equipped with a series of adjustable screws. The two inlet walls were placed 2.5 cm deep from the top of the upper MS1 layer, in the middle of the container, with a spacing of 1.5 cm. The sand in the container was packed under water saturated conditions to avoid any entrapped air between the sand particles. The flow container was initially filled halfway with water and then, after having thoroughly mixed the sand with water in another container, the sand was gradually poured into the flow container. To maintain a fully water saturated system during packing, a water head over the top layer of the sand was kept at all times. At each filling step, each sand layer was tamped in the same manner to compact the porous medium. To prevent accumulation of sand in the bottom valve, a nylon filter was put in the bottom port.

To create partially water saturated conditions in the sand-filled container, the system was drained from the bottom. After having allowed the water phase to achieve an equilibrium configuration (24 h after the partial drainage of the system), a trench of 1.5 cm width and 6 cm depth, with vertical walls, was carefully excavated between the inlet screens (Fig. 1, right), thus creating additional space for the $Hg^0$

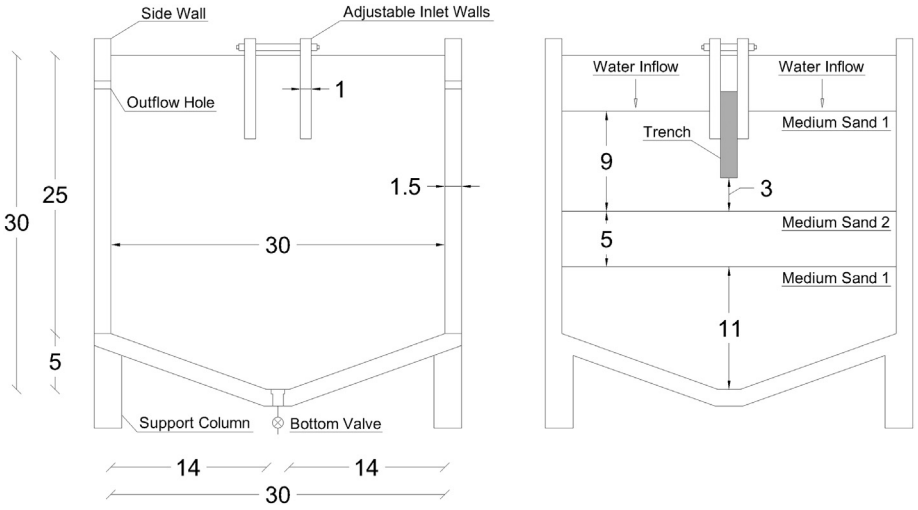


**Fig. 1.** Flow container (left) and system (right) details (dimensions in cm). Liquid $Hg^0$ in grey.

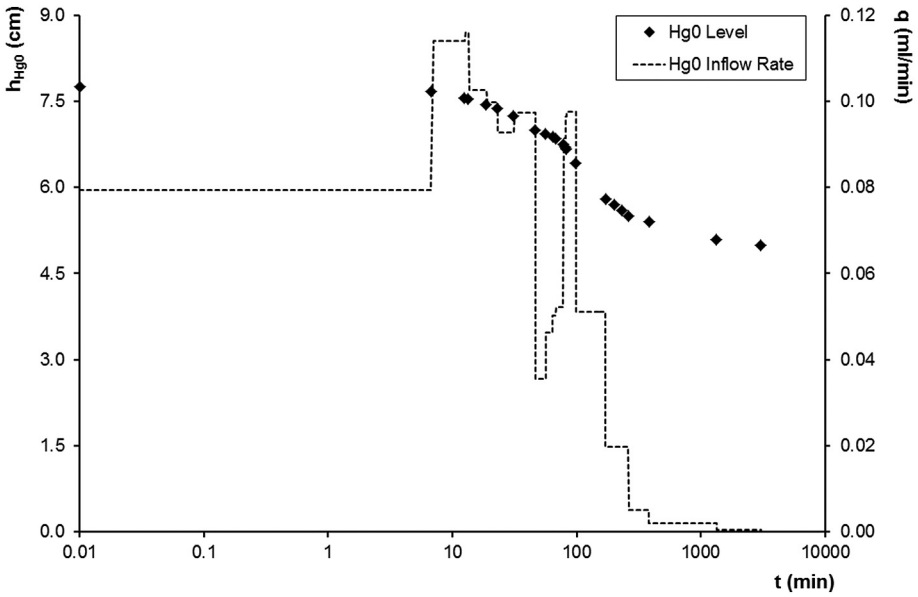


**Fig. 2.** Measured $Hg^0$ inflow rate and level in the reservoir over time - Stage 1.

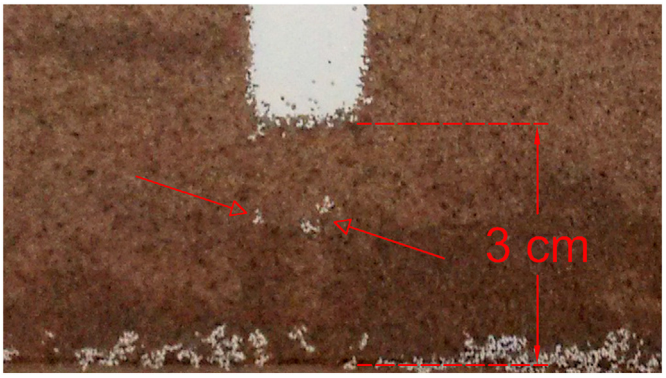


**Fig. 3.** Detail of $Hg^0$ distribution below the reservoir with red arrows indicating the two fingers - End of stage 1. (For interpretation of the references to colour in this figure legend, the reader is referred to the web version of this article.)

DNAPL reservoir. This made it possible to observe whether $Hg^0$ lateral spreading from the reservoir would occur.

The flow container experiment consisted of two stages. In the first stage, liquid $Hg^0$ was carefully added in the trench in five steps, of about 9.2 ml each, until the DNAPL built enough head to infiltrate and migrate within the partially water saturated system. The second stage of the experiment consisted of the simulation of a "rain event" to assess whether the elemental mercury already infiltrated within the system could be mobilized due to local increases in water saturation. The rain event lasted 40 min and was performed by pouring water on top of the upper MS1 layer with two sources, of 2.5 ml/min each, placed in the middle of each portion outside the inlet walls (Fig. 1). During the entire experiment, the $Hg^0$ level in the reservoir and its infiltration front were tracked with a camera to determine its infiltration rate and its position over time within the system. Visual and camera observations allowed to determine when $Hg^0$ migration ceased and equilibrium was achieved. Equilibrium was assumed when no visible changes in the $Hg^0$ front were noticeable in the recorded images.

### 2.3. Porosity and fluid saturations measurements

Non-intrusive measurements of porosity, water and $Hg^0$ saturations were performed over the whole system with a dual gamma ray apparatus (D'Aniello, 2017; D'Aniello et al., 2018b), consisting of two

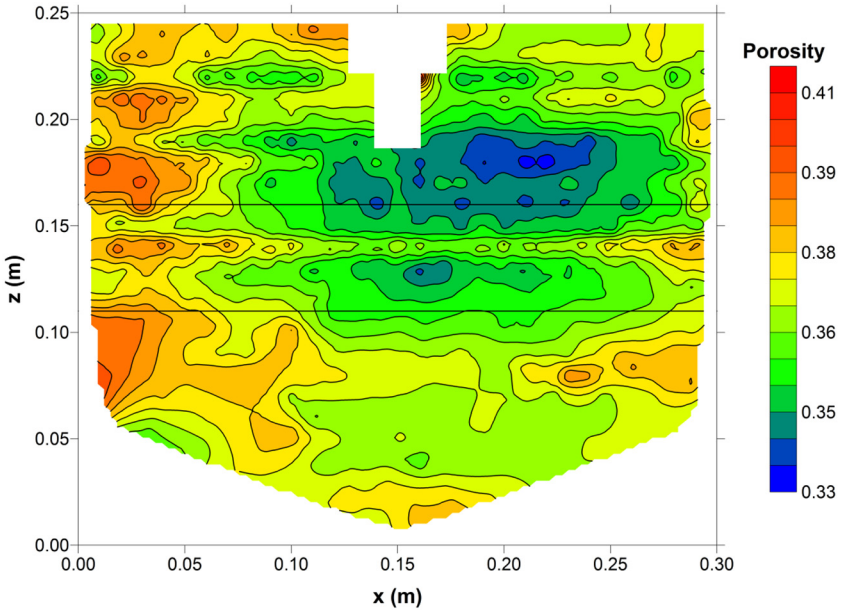


**Fig. 4.** Measured porosity field.

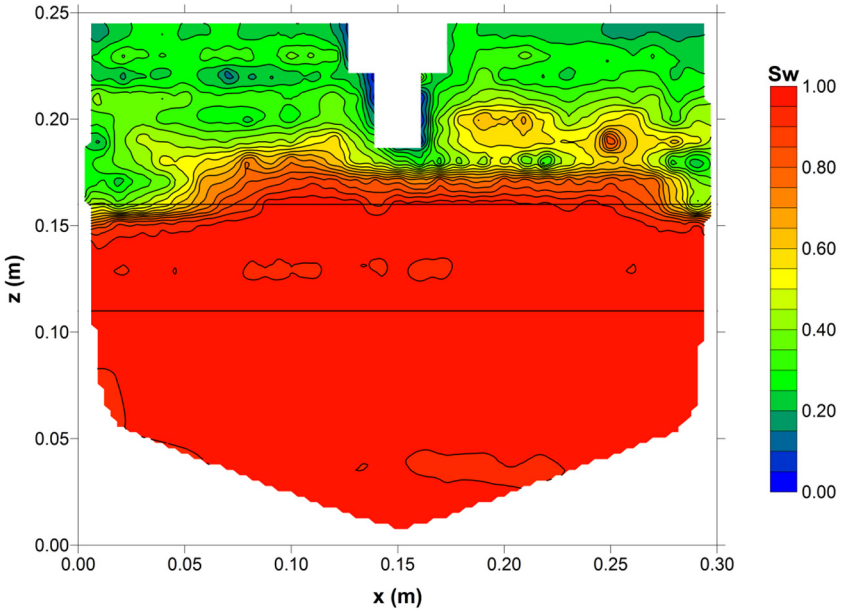


**Fig. 5.** Measured initial water saturation ($S_w$) profile.

radioactive sources, namely Americium 241 ($^{241}$Am) and Cesium 137 ($^{137}$Cs), and a sodium iodide (NaI) detector. The measurements were made over a regular grid of 632 points with 1 cm spacing. The porosity field was measured first, at the end of the packing procedure, when the system was fully water saturated. Then, when the system was drained, the initial water saturation distribution was determined after the trench excavation. Liquid $Hg^0$ and water saturation profiles were measured 24 h after the end of each experimental stage (sec. 2.2), established when there was no further change in the liquid $Hg^0$ level in the trench.

## 3. Results and discussion

### 3.1. Flow container experiment: stage 1

During the first stage of the flow container experiment, liquid $Hg^0$ infiltration and distribution occurred in the partially water saturated stratified sand under an observed DNAPL head of 7.76 cm. Infiltration of $Hg^0$ took place directly at the bottom of the trench, with no evidence of lateral spreading until the MS2 layer was encountered. A volume of 16.3 ml of elemental mercury infiltrated within the system. Infiltration stopped after 50.9 h (3054 min), and the $Hg^0$ level in the reservoir reached the final value of 5 cm. The $Hg^0$ inflow rate did not show a clear trend over time (Fig. 2), other than highest infiltration rates occurring in the first 2 h.

As observed for the infiltration of other DNAPLs (Kueper and Gerhard, 1995), the fluctuations reported in the elemental mercury inflow rate were likely induced by the heterogeneities present within the porous formation. Another factor that probably increased these variations was the spatial and temporal variability of the water saturation field as $Hg^0$ infiltrated and distributed within the system. D'Aniello et al. (2018a) observed that $Hg^0$ migration in partially water saturated porous media is followed by a redistribution of water within

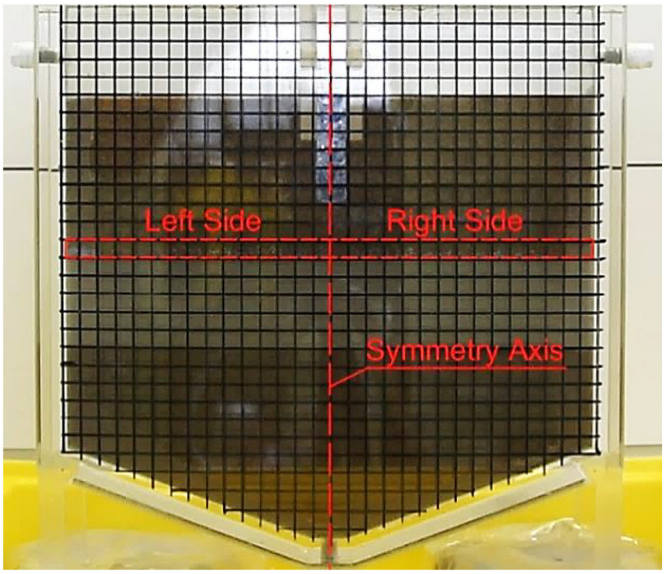


**Fig. 6.** Detail of the $Hg^0$ lateral spreading zone (dashed rectangular box).

the pores, hence of air. As elemental mercury is nonwetting with respect to air, the variation over time of the air saturation within the pores probably affected $Hg^0$ migration, as well as its infiltration pattern.

Infiltration of liquid $Hg^0$ into MS1 occurred when raising the DNAPL level in the trench from 6.21 cm to 7.76 cm. This is significantly lower (25.7–40.6%) than the DNAPL entry head of 10.45 cm (Table 3; D'Aniello et al., 2018a) observed in the $P_c(S)$ experiment under stable flow behaviour for this sand. Moreover, this lower entry head occurred despite both average porosity (0.344) and water saturation (0.240), in the first centimetre beneath the trench, were about 4% and 2.5 times lower than in the $P_c(S)$ experiment. A reduction in porosity (hence, likely, in intrinsic permeability) and in water saturation would be expected to yield higher rather than lower entry heads. Probably, $Hg^0$ infiltrated thanks to the presence of locally larger pores, but its migration through the upper layer of MS1 was possible because of the triggering of gravity induced instabilities, like fingering (Homsy, 1987; Kueper and Frind, 1988; Illangasekare et al., 1995a, 1995b; Mayer and Hassanizadeh, 2005).

Initially, the static DNAPL head available in the trench was sufficient to allow $Hg^0$ to overcome the entry head dictated by the locally present heterogeneities, and the effect of gravity likely induced an infiltration through preferential pathways rather than through a uniform front. Visual observations further suggested this, indicating that at least two fingers might have developed (Fig. 3). Integration of dual gamma ray measurements over the 2 cm below the reservoir may also help suggesting this hypothesis. At the end of the first stage of the experiment, only 2% of the total pore volume in the 2 cm below the reservoir was occupied by liquid mercury, based on a measured average porosity of 0.345 and a liquid $Hg^0$ volume of about 0.08 ml. Therefore, based on such a small volume, it is likely that $Hg^0$ migration occurred through preferential pathways. Since lateral spreading occurred on top of MS2, elemental mercury was also likely continuous beneath the reservoir, thus providing a connection with the DNAPL source in the trench.

Elemental mercury reached the top of the MS2 layer in about 9 min, when a volume of 0.79 ml of liquid $Hg^0$ had infiltrated, based on the measured inflow rate (Fig. 2). The dual gamma ray measurements (Figs. 4 and 8) performed at the end of the first stage of the experiment indicated that 0.69 ml of liquid $Hg^0$ infiltrated in the first 3 cm beneath the trench. The comparison of the volume obtained by integration of the dual gamma ray measurements with that calculated based on the measured inflow rate suggests that, in the first 3 cm below the DNAPL reservoir, most of the elemental mercury infiltrated in the first minutes of the experiment, and that no significant changes were observed at later times. Therefore, once mercury found a pathway from the DNAPL source in the trench down to the bottom of the upper MS1 layer, all the additional infiltrated $Hg^0$ probably migrated through this pathway before distributing on top of the MS2 layer.

Including the 3 cm of DNAPL head below the bottom of the trench (Fig. 3), the total liquid $Hg^0$ head on top of the MS2 layer was at maximum 10.5 cm, according to the mercury level in the reservoir (Fig. 2). However, this head was not sufficient to allow liquid $Hg^0$ to penetrate MS2. This is in keeping with the higher entry heads found under stable flow behaviour for $Hg^0$ in this sand (Table 3; D'Aniello et al., 2018a), in both fully (12.51 cm) and partially water saturated conditions (15.74 cm). No infiltration via fingers occurred in MS2 as its narrower particle size distribution and lower particles sizes than MS1 (Table 1) likely prevented mercury from invading even a single pore of this layer. Therefore, elemental mercury found easier pathways to continue its infiltration into the upper MS1 layer, thus distributing on

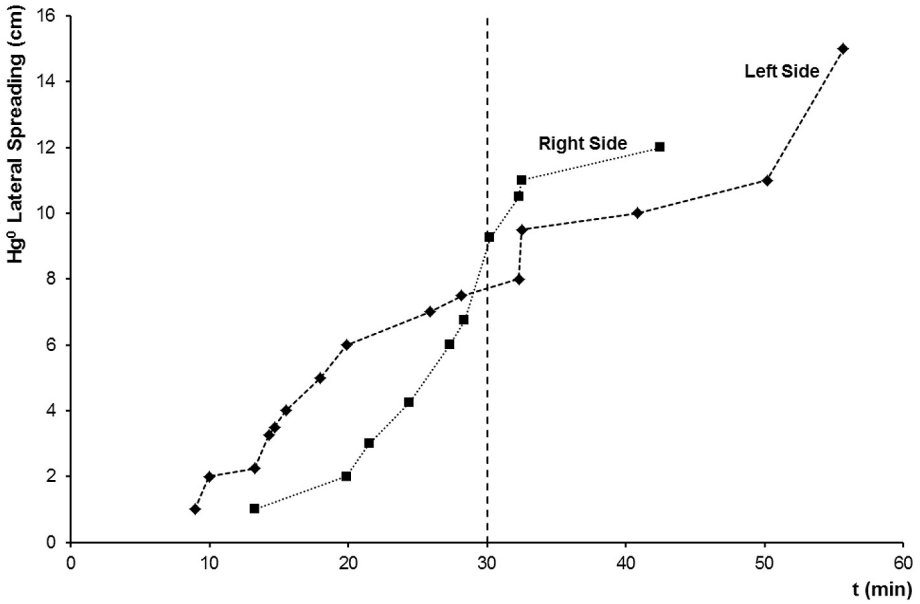


**Fig. 7.** Measured $Hg^0$ lateral spreading above the MS2 layer on both left and right sides with respect to the vertical symmetry axis.

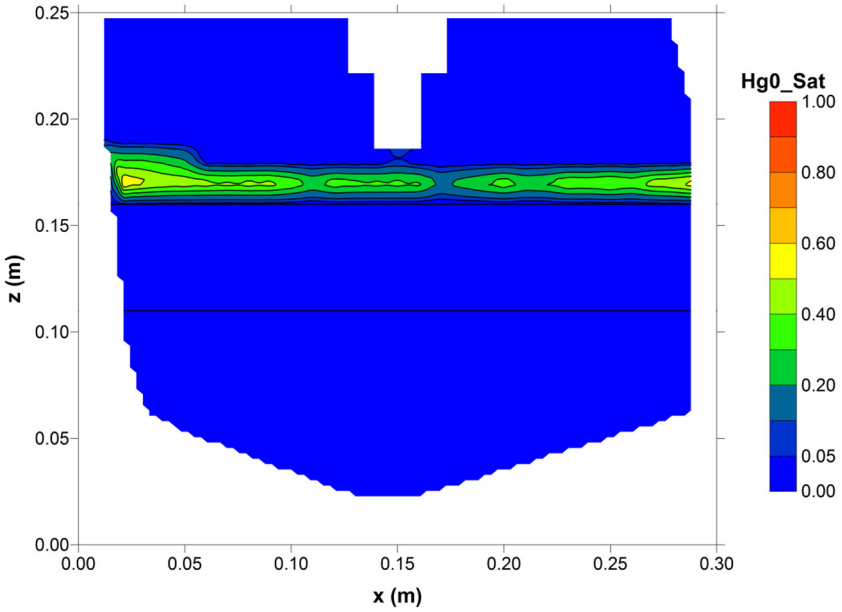


**Fig. 8.** Measured $Hg^0$ saturation profile - End of stage 1.

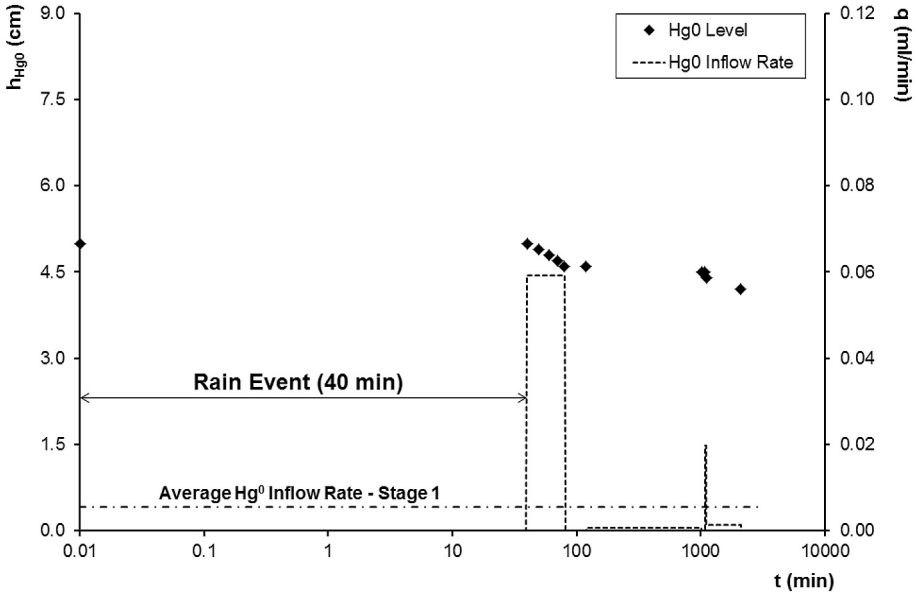


**Fig. 9.** Measured $Hg^0$ inflow rate and level in the reservoir over time - Stage 2. The average $Hg^0$ inflow rate of stage 1 is also reported (dashed-dotted line).

top of the MS2 layer.

Once mercury reached the top of MS2, it created a pool of about 1 cm height. Elemental mercury distribution over MS2 was not symmetric (Figs. 6 and 7), and the infiltration front was initially faster on the left side because of the higher porosity, hence higher intrinsic permeability, found (Fig. 4), since water saturation was practically the same in the first 6–7 cm on both sides of the lateral spreading zone above MS2 (Fig. 5). This trend reversed after 30 min (Fig. 7) because of the lower water saturation found at the left side (Fig. 5) as a result of the higher porosity (Fig. 4). The larger the pores, the lower the entry head, so air easily filled this part of the system, thus locally dampening the infiltration, as $Hg^0$ is nonwetting with respect to air and is required to overcome higher entry heads due to its presence (Table 3; D'Aniello et al., 2018a). Then, at about 42 min, the infiltration temporarily ceased on the right side, even though the water saturation was nearly the same at the $Hg^0$ front locations, and the higher porosity on the left side allowed liquid mercury to infiltrate easier and faster through this part of the system (Fig. 7). Therefore, the effect induced by the heterogeneity of the porous medium structure likely prevailed in determining a preferential pathway for liquid $Hg^0$ infiltration and distribution. The inspection of Fig. 8 further suggests this, thus showing a tendency of liquid $Hg^0$ to migrate towards the left side of the container, where porosity was the highest (0.392) above the MS2 layer, as well as the $Hg^0$ saturation (0.615), and the height of the DNAPL pool increased to 2 cm.

### 3.2. Flow container experiment: stage 2 - "rain event"

The second stage of the flow container experiment consisted of the simulation of a "rain event", to test whether redistribution of the liquid $Hg^0$ present within the system could be induced by local increases in water saturation. The increase in water saturation of the system induced the infiltration of a significant additional volume of 4.7 ml of elemental mercury, for a total of 21 ml. Infiltration stopped after 35 h (2100 min), and the $Hg^0$ level in the trench reached the final value of

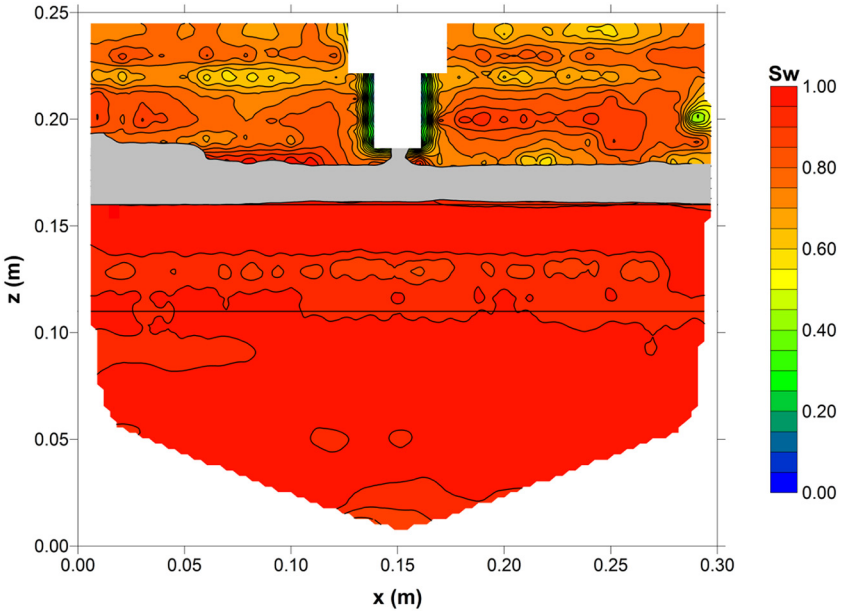


**Fig. 10.** Measured water saturation ($S_w$) profile (in grey the $Hg^0$ distribution) - End of stage 2.

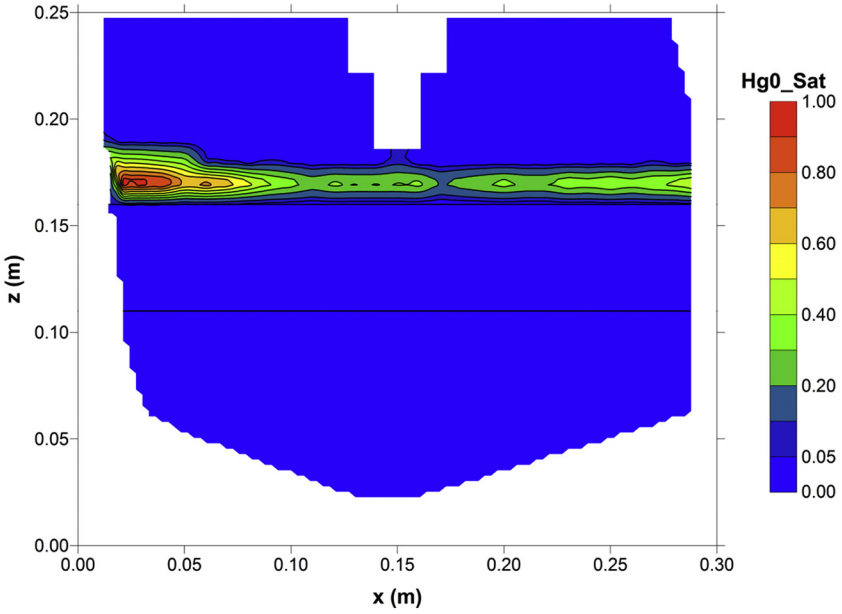


**Fig. 11.** Measured $Hg^0$ saturation profile - End of stage 2.

4.2 cm (Fig. 9). The mobilization of the liquid $Hg^0$ present within the system occurred at the end of the rain event, after 40 min, when the additional water, infiltrated from the top, almost completely saturated the MS1 layer above MS2 (Fig. 10).

During stage 2, the infiltration of elemental mercury mostly occurred in the first 40 min following the end of the rain event (Fig. 9). In this time interval, the $Hg^0$ inflow rate reached its maximum value ($0.592 \cdot 10^{-1}$ ml/min; Fig. 9), of about half of the maximum rate measured during stage 1 (0.116 ml/min; Fig. 2) but of about one order of magnitude higher than the average inflow rate of stage 1 ($0.536 \cdot 10^{-2}$ ml/min; Fig. 9). Both inflow rate and DNAPL level in the trench showed a stepwise pattern over time (Fig. 9), with large time intervals where no (or negligible) liquid $Hg^0$ infiltration occurred. This may be explained based on the time required for water to redistribute within the system. As water slowly imbibed the pores, a displacement of air occurred, allowing further elemental mercury infiltration.

The mobilization of elemental mercury was likely dictated by the local increase of the water saturation up to values near to unity (Fig. 10), since the $Hg^0$ entry head is lower in a fully rather than in a partially water saturated porous medium (Table 3; D'Aniello et al., 2018a). Dual gamma ray measurements showed no considerable changes in the shape of the $Hg^0$ front at the end of stage 2 (Fig. 11) compared to the final distribution at the end of stage 1 (Fig. 8). The additional volume of elemental mercury mainly moved within the areas of the system where it already infiltrated before the rain event (stage 1), thus locally increasing the DNAPL saturation (Fig. 11). As for the first stage of the experiment, the heterogeneity in the porosity field (hence in the intrinsic permeability field) likely had a crucial role in determining the $Hg^0$ redistribution pathway. Liquid mercury mainly moved towards the left side of the system, where porosity was the highest above MS2 (Fig. 4). In particular, $Hg^0$ reached a saturation almost equal to unity in the left side of the system (Fig. 11), as confirmed

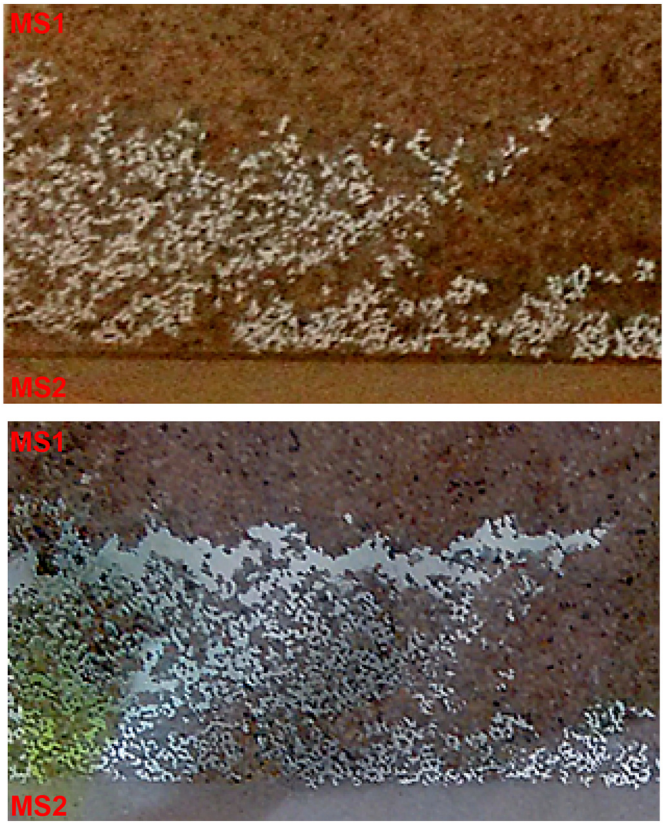


**Fig. 12.** Detail of the $Hg^0$ (re)distribution front in proximity of the left side wall at the end of stage 1 (top) and stage 2 (bottom).

by the visual observation of a local thickening of its redistribution front (Fig. 12).

These last experimental results provide evidence that, if liquid $Hg^0$ infiltration occurs within a partially water saturated system, in contrast with other NAPLs (Yang et al., 2013) the extent and the magnitude of its migration can considerably increase when the water saturation increases and reaches values near to unity. For example, if $Hg^0$ DNAPL is present in a ditch or in wastes buried in the unsaturated zone, an increase in the water saturation, induced by a groundwater table rise, prolonged and intense rains, or flooding, may cause elemental mercury to remobilize and infiltrate deeper in the subsurface. Moreover, if the mercury DNAPL is still connected within the porous formation with the original source of contamination from which it infiltrated, it has a head and volume contribution readily available to feed further infiltration once the water saturation increases where the $Hg^0$ infiltration front previously stopped and reached equilibrium.

This study further enforces the previous findings of D'Aniello et al. (2018a), stressing the importance of the effects of the variation in water saturation on $Hg^0$ DNAPL infiltration and distribution in variably water saturated porous media. Thanks to its extraordinary high surface tension (Table 2), liquid elemental mercury shows a different infiltration and distribution behaviour with respect to well-known DNAPLs, and the conventional wettability hierarchy, in which the NAPL is intermediate wetting between air and water, cannot stand for elemental mercury. Therefore, more physical knowledge is required to formulate a new constitutive model able to describe elemental mercury DNAPL infiltration and distribution behaviour in variably water saturated porous media. In particular, experimental investigations at the pore level would be beneficial to assess whether a wettability hierarchy exists between liquid $Hg^0$, air, and water, and what happens when these three phases interact between each other within a porous medium.

## 4. Conclusions

The flow container experiment presented in this study demonstrated that, under conditions similar to those found in the field, $Hg^0$ DNAPL infiltration is likely to occur via fingers and is strongly controlled by porous medium structure and water saturation. As elemental mercury is nonwetting with respect to air, the presence of air within the pores locally dampened its infiltration and distribution. However, the effect induced by the heterogeneity of the porous medium structure likely prevailed in determining a preferential pathway for liquid $Hg^0$ infiltration and distribution. Dual gamma ray measurements further suggested this as elemental mercury was found in higher saturations where porosity was higher.

The experiment further showed that, if liquid $Hg^0$ infiltration occurs within a partially water saturated system, the extent and the magnitude of its migration can considerably increase when the water saturation increases up to values near to unity and the mercury DNAPL already infiltrated is still connected with the original source of contamination. In field scenarios, a groundwater table rise, prolonged and intense rains, or flooding may cause elemental mercury to remobilize and infiltrate deeper if it is present in the unsaturated zone.

## Acknowledgements

This research was financially supported by the P.O.R. Campania FSE 2007/2013-2014/2020.

## References

Adamson, A.W., Gast, A.P., 1997. Physical Chemistry of Surfaces, 6Ed. Wiley.
Arbestain, M.C., Rodriguez-Lado, L., Bao, M., Macias, F., 2009. Assessment of mercury-polluted soils adjacent to an old mercury-fulminate production plant. Appl. Environ. Soil Sci. 2009 8.
Bear, J., 1972. Dynamics of Fluids in Porous Media. Dover Publications, Inc, New York.
Bernaus, A., Gaona, X., van Ree, D., Valiente, M., 2006. Determination of mercury in polluted soils surrounding a chlor-alkali plant: direct speciation by X-ray absorption spectroscopy techniques and preliminary geochemical characterisation of the area. Anal. Chim. Acta 565 (1), 73–80.
Biester, H., Müller, G., Schöler, H.F., 2002. Estimating distribution and retention of mercury in three different soils contaminated by emissions from chlor-alkali plants: part I. Sci. Total Environ. 284 (1), 177–189.
Bollen, A., Wenke, A., Biester, H., 2008. Mercury speciation analyses in $HgCl_2$-contaminated soils and groundwater - implications for risk assessment and remediation strategies. Water Res. 42 (1), 91–100.
Brooks, S.C., Southworth, G.R., 2011. History of mercury use and environmental contamination at the Oak Ridge Y-12 Plant. Environ. Pollut. 159 (1), 219–228.
Compeau, G.C., Bartha, R., 1985. Sulfate-reducing bacteria: principal methylators of mercury in anoxic estuarine sediment. Appl. Environ. Microbiol. 50 (2), 498–502.
CRC, 2014. Handbook of Chemistry and Physics, 94th ed. (Internet Version 2014).
D'Aniello, A., 2017. The flow behaviour of elemental mercury DNAPL in porous media. In: Università degli Studi di Napoli Federico II, https://doi.org/10.6093/UNINA/FEDOA/11617.
D'Aniello, A., Hartog, N., Sweijen, T., Pianese, D., 2018a. Infiltration behaviour of elemental mercury DNAPL in fully and partially water saturated porous media. J. Contam. Hydrol. 209, 14–23. https://doi.org/10.1016/j.jconhyd.2018.01.001.
D'Aniello, A., Hartog, N., Sweijen, T., Pianese, D., 2018b. Infiltration and distribution of elemental mercury DNAPL in water-saturated porous media: experimental and numerical investigation. Water Air Soil Pollut. 229 (1), 25. https://doi.org/10.1007/s11270-017-3674-0.
Davis, A., Bloom, N.S., Que Hee, S.S., 1997. The environmental geochemistry and bioaccessibility of mercury in soils and sediments: a review. Risk Anal. 17 (5), 557–569.
Deeb, R., Hawley, E., Kell, L., O'Laskey, R., 2011. Assessing alternative endpoints for groundwater remediation at contaminated sites. In: ESTCP-Project ER-200832.
Devasena, M., Nambi, I.M., 2010. Migration and entrapment of mercury in porous media. J. Contam. Hydrol. 117, 60–70.
FILCOM-Sibelco Group, 2015. Technical Datasheet Filtersand 0.2–0.5 mm and Silversand S60.
Gilmour, C.C., Henry, E.A., Mitchell, R., 1992. Sulfate stimulation of mercury methylation in freshwater sediments. Environ. Sci. Technol. 26 (11), 2281–2287.
Golder Associates, 2011. 2010 *Conceptual Site Model - Botany*. Report No. 107623162_001_R_Rev0.
González-Fernández, B., Menéndez-Casares, E., Meléndez-Asensio, M., Fernández-Menéndez, S., Ramos-Muñiz, F., Cruz-Hernández, P., González-Quirós, A., 2014. Sources of mercury in groundwater and soils of west Gijón (Asturias, NW Spain). Sci. Total Environ. 481, 217–231.
Homsy, G.M., 1987. Viscous fingering in porous media. Annu. Rev. Fluid Mech. 19 (1),

271–311.
Hylander, L.D., Meili, M., 2003. 500 years of mercury production: global annual inventory by region until 2000 and associated emissions. Sci. Total Environ. 304 (1), 13–27.
Illangasekare, T.H., Ramsey Jr., J.L., Jensen, K.H., Butts, M.B., 1995a. Experimental study of movement and distribution of dense organic contaminants in heterogeneous aquifers. J. Contam. Hydrol. 20 (1–2), 1–25.
Illangasekare, T.H., Armbruster III, E.J., Yates, D.N., 1995b. Non-aqueous-phase fluids in heterogeneous aquifers-experimental study. J. Environ. Eng. 121 (8), 571–579.
ITRC, 2012. Using Remediation Risk Management to Address Groundwater Cleanup Challenges at Complex Sites. pp. 31.
Kueper, B.H., Frind, E.O., 1988. An overview of immiscible fingering in porous media. J. Contam. Hydrol. 2 (2), 95–110.
Kueper, B.H., Gerhard, J.I., 1995. Variability of point source infiltration rates for two-phase flow in heterogeneous porous media. Water Resour. Res. 31 (12), 2971–2980.
Lechler, P.J., Miller, J.R., Lacerda, L.D., Vinson, D., Bonzongo, J.C., Lyons, W.B., Warwick, J.J., 2000. Elevated mercury concentrations in soils, sediments, water, and fish of the Madeira River basin, Brazilian Amazon: a function of natural enrichments? Sci. Total Environ. 260 (1), 87–96.
Leterme, B., Jacques, D., 2013. Literature review on mercury speciation soil systems under oxidizing conditions. In: Snowman Network, IMaHG Report, Project No. SN-03/08.
Leterme, B., Blanc, P., Jacques, D., 2014. A reactive transport model for mercury fate in soil-application to different anthropogenic pollution sources. Environ. Sci. Pollut. Res. 21 (21), 12279–12293.
Mayer, A., Hassanizadeh, S.M., 2005. Soil and groundwater contamination: nonaqueous phase liquids, principles and observations. In: Water Resources Monograph 17. American Geophysical Union.
Miller, C.L., Watson, D.B., Lester, B.P., Lowe, K.A., Pierce, E.M., Liang, L., 2013. Characterization of soils from an industrial complex contaminated with elemental mercury. Environ. Res. 125, 20–29.
NICOLE, 2015. Risk-based management of mercury-impacted sites. In: Network for Industrially Contaminated Land in Europe.
Pasha, A.Y., Khoshghalb, A., Khalili, N., 2015. Pitfalls in interpretation of gravimetric water content-based soil-water characteristic curve for deformable porous media. Int. J. Geomech. 16 (6), D4015004.
Pirrone, N., Cinnirella, S., Feng, X., Finkelman, R.B., Friedli, H.R., Leaner, J., Mason, R., Mukherjee, A.B., Stracher, G.B., Streets, D.G., Telmer, K., 2010. Global mercury emissions to the atmosphere from anthropogenic and natural sources. Atmos. Chem. Phys. 10 (13), 5951–5964.
Risher, J.F., 2003. Elemental mercury and inorganic mercury compounds: human health aspects. In: Concise International Chemical Assessment Document. World Health Organization, Geneva.
Scanlon, B.R., Tachovsky, J.A., Reedy, R., Nicot, J.P., Keese, K., Slade, R.M., Merwad, V., Howard, M.T., Wells, G.L., Mullins, G.J., Ortiz, D.M., 2005. Groundwater–surface water interactions in Texas. In: Implications for Water Resources and Contaminant Transport (TCEQ), Bureau of Economic Geology. The University of Texas, Austin, pp. 129–131.
Sillers, W.S., Fredlund, D.G., Zakerzadeh, N., 2001. Mathematical attributes of some soil-water characteristic curve models. In: Unsaturated Soil Concepts and Their Application in Geotechnical Practice. Springer, Netherlands, pp. 243–283.
Sweijen, T., Hartog, N., Marsman, A., Keijzer, T.J., 2014. The transport behaviour of elemental mercury DNAPL in saturated porous media: analysis of field observations and two-phase flow modelling. J. Contam. Hydrol. 161, 24–34.
Sznopek, J.L., Goonan, T.G., 2000. The materials flow of mercury in the economies of the United States and the world. US Geol. Surv (Circular 1197) 32 pages.
UNEP, 2002. Global Mercury Assessment. Geneva, Switzerland.
US DOE, 2001. *Mercury Contaminated Material Decontamination Methods: Investigation and Assessment*. DE-FG21-95EW55094.
US EPA, 2007. *Treatment Technologies for Mercury in Soil, Waste, and Water*. EPA Report 542-R-07-003. US Environmental Protection Agency, Office of Superfund Remediation and Technology Innovation.
Walvoord, M.A., Andraski, B.J., Krabbenhoft, D.P., Striegl, R.G., 2008. Transport of elemental mercury in the unsaturated zone from a waste disposal site in an arid region. Appl. Geochem. 23 (3), 572–583.
World Chlorine Council, 2011. Reduction of mercury emissions and use from the chlor-alkali sector partnership.
Yang, Z., Zandin, H., Niemi, A., Fagerlund, F., 2013. The role of geological heterogeneity and variability in water infiltration on non-aqueous phase liquid migration. Environ. Earth Sci. 68 (7), 2085–2097.